This article has been accepted for publication in a future issue of this journal, but has not been fully edited. Content may change prior to final publication. Citation information: DOI 10.1109/TPEL.2014.2304677, IEEE Transactions on Power Electronics

One dimensional spectral analysis of complex PWM waveforms using superposition

Toit Mouton (IEEE Member)

Department of Electrical and Electronic Engineering

University of Stellenbosch

Private Bag X1, Matieland, 7602

South Africa

Email: dtmouton@sun.ac.za

Brendan McGrath (IEEE member)

Grahame Holmes (IEEE Fellow)

Richardt Wilkinson (IEEE senior member)

School of Electrical and Computer Engineering

RMIT University

Melbourne

Australia

Email: brendan.mcgrath@rmit.edu.au

Abstract

This paper takes a new look at the mechanisms underlying the double-edge pulse-width modulation (PWM) process. It presents a novel way of deriving equations for the spectrum of double-edge PWM using basic mathematical techniques. In the process the underlying non-linearities that generate the PWM sidebands are identified. Unlike the classical double Fourier series approach, the proposed method of deriving the PWM spectrum does not require the construction of the so-called unit cell. The interaction between this new model of the pulse-width modulator and the regular sampling process is studied and generalized equations for the Fourier transforms of regularly sampled PWM waveforms are derived. A general solution to the important question of what happens to the PWM spectrum when the PWM reference consists of a summation of signals is presented. It is shown that the addition of reference signals in the time domain results in a double convolution of the PWM sidebands in the frequency domain. As an application of this result, it is shown how new analytic equations for the harmonics of third harmonic injection PWM and space vector modulation can easily be derived. Finally, the new theoretical results are benchmarked against results from the well-established double Fourier series method.

Index Terms

Carrier based PWM strategies, third harmonic injection, space vector modulation, double Fourier integral, Pulse-width modulation, Regular sampling, superposition

This article has been accepted for publication in a future issue of this journal, but has not been fully edited. Content may change prior to final publication. Citation information: DOI 10.1109/TPEL.2014.2304677, IEEE Transactions on Power Electronics

I. Introduction

Pulse-width modulation (PWM) is fundamental to power electronics and has been a major research area for more than four decades. Sinusoidal pulse-width modulation (SPWM) has been studied since the 1950's. The first analysis of the harmonics generated by naturally-sampled sinusoidal pulse-width modulation can be found in [1]. The geometric model presented in this textbook is an innovative application of periodic waveforms of two variables and was based on work of Bennett [2]. Other approaches to calculating the PWM spectrum have been reported [3]–[8], but this original method of deriving a double Fourier series expansion for the PWM pulse train has since become the basis on which most further research is based.

Another approach to calculating the PWM spectrum is to combine Fast Fourier Transform (FFT) techniques with simple time-domain simulations of the switched waveform. However, this approach suffers from several drawbacks. The simulation time steps must be very small in order to obtain a low enough noise floor to make meaningful conclusions. The problem becomes more severe if the carrier-to-fundamental frequency ratio is not an integer in which case the time-domain simulation has to run over a number of fundamental cycles. It also leaves the uncertainty as to whether a small simulation error has tarnished the results which happens quite easily [9].

On the other hand the analytical solutions derived from the double Fourier series method provide accurate results as well as considerable insight beyond what can be achieved by using basic FFT techniques. It makes it possible to accurately compare different modulation strategies, provides the theoretical base for understanding how harmonics cancel when using phase-shifted carriers [10] and leads to a fundamental understanding of the natural balancing mechanisms of multilevel converters [11]–[18].

The classical and well-established analytic method of Bennett and Black starts with the construction of the two-dimensional unit cell from the PWM reference signal. This step requires a certain amount of geometric insight and a new unit cell has to be constructed for every reference signal. The next step is to expand the resulting function of two variables into its two-dimensional Fourier series. This requires the calculation of complex double integrals which may become extremely challenging and time consuming, for instance in the case of space vector modulation [9]. The final step is to substitute these equations for the double Fourier coefficients back into the double Fourier series expansion which results in an expansion for the harmonics of the PWM waveform. Special mathematical tricks have been developed to modify this technique in the case of regular sampled PWM. However, these tricks provide little insight into the sampling process and its interaction with the pulse-width modulator. Another disadvantage is the fact that the integration limits have to be modified and the double integrals re-evaluated for every sampling method.

In [19] a different approach to analyzing the PWM spectrum of single-edge modulation was introduced. Using elementary mathematical techniques it was shown how the PWM pulse train consists of the superposition of the reference, the sawtooth carrier and a sawtooth term with a phase modulation caused by the carrier. It was further shown that superposition of reference signals in the time domain results in a convolution of the respective sidebands in the frequency domain. The interaction between the sampling process and the pulse width modulator was studied and a general equation for the Fourier transform of the PWM pulse train for regularly sampled PWM was developed. The techniques in [19] can be used to analyze the PWM spectrum for both periodic and a-periodic reference signals. The current paper extends the analysis developed in [19] to double-edge PWM.

Section II provides a brief review of the strategy proposed in [19]. In section III it is shown how the double-edge modulator can be represented by two single-edge modulators. Sinusoidal modulation is studied in section VI. Section VII answers a fundamental question by showing that the addition of reference waveforms in the time-domain corresponds to a double convolution of the respective sidebands in the frequency domain. In section VIII it is shown how this powerful theorem

This article has been accepted for publication in a future issue of this journal, but has not been fully edited. Content may change prior to final publication. Citation information: DOI 10.1109/TPEL.2014.2304677, IEEE Transactions on Power Electronics

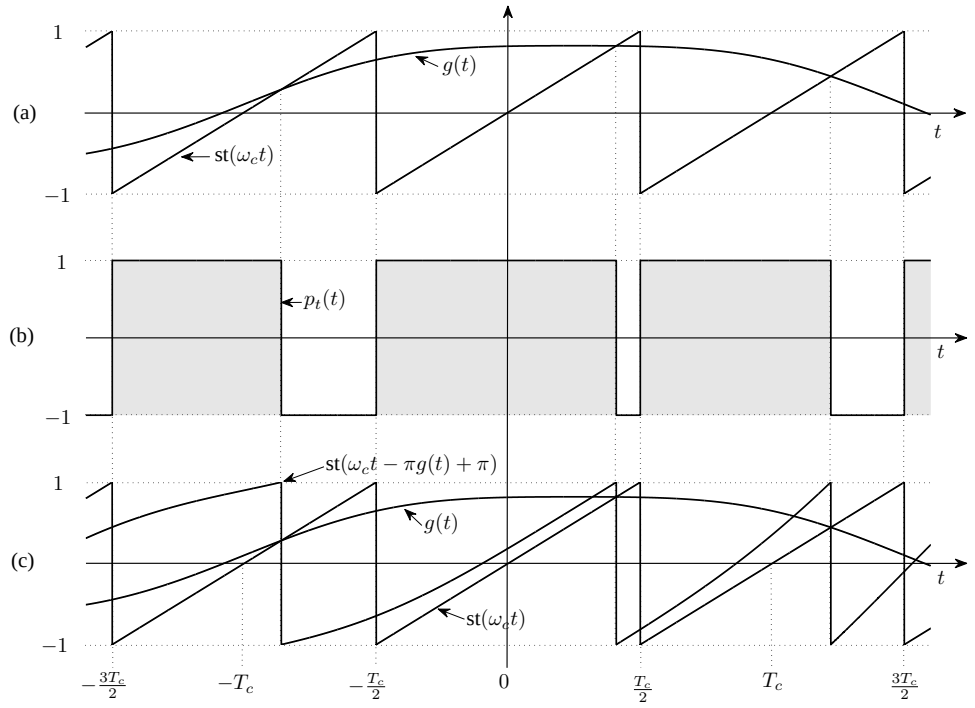

Fig. 1. Expanding the trailing edge PWM pulse train into sawtooth functions.

significantly simplifies the derivation of analytic equations for the PWM spectra for third harmonic injection and space vector modulation. Finally, in section IX, the analytic results from this paper are benchmarked against those calculated through the classical double Fourier series method as well as the results of time-domain simulations.

II. Review of Single-Edge Modulation

Consider the trailing-edge naturally sampled PWM pulse train $p_t(t)$ in Fig. 1(b) generated by comparing the PWM reference waveform $g(t)$ with the sawtooth carrier $\text{st}(\omega_c t)$ of Fig. 1(a), where ω_c is the switching frequency and $T_c = \frac{2\pi}{\omega_c}$ is the switching period. In [19] elementary mathematical techniques were used to show that this pulse train can be decomposed as the sum of three functions

$$p_t(t) = g(t) - \text{st}(\omega_c t) + \text{st}(\omega_c t - \pi g(t) + \pi), \tag{1}$$

as shown in Fig. 1(c). It shows that the PWM pulse train is the superposition of the reference, the carrier and a sawtooth term with phase modulation caused by the reference $g(t)$.

The next step in [19] was to to expand the sawtooth function $\text{st}(\theta)$ into its exponential Fourier series representation:

$$\text{st}(\theta) = \frac{j}{\pi} \sum_{\substack{m=-\infty \\ m\neq 0}}^{\infty} \frac{e^{jm(\theta+\pi)}}{m} \tag{2}$$

Note that the symbol $\sum_{\substack{m=-\infty \\ m\neq 0}}^{\infty}$ indicates the sum as m ranges from $-\infty$ to ∞, excluding the case $m = 0$.

Replacing the second sawtooth function in Eq. (1) with its Fourier series expansion results in

$$p_t(t) = g(t) - \text{st}(\omega_c t) + \frac{j}{\pi} \sum_{\substack{m=-\infty \\ m\neq 0}}^{\infty} \frac{1}{m} e^{jm(\omega_c t - \pi g(t))}. \tag{3}$$

This article has been accepted for publication in a future issue of this journal, but has not been fully edited. Content may change prior to final publication. Citation information: DOI 10.1109/TPEL.2014.2304677, IEEE Transactions on Power Electronics

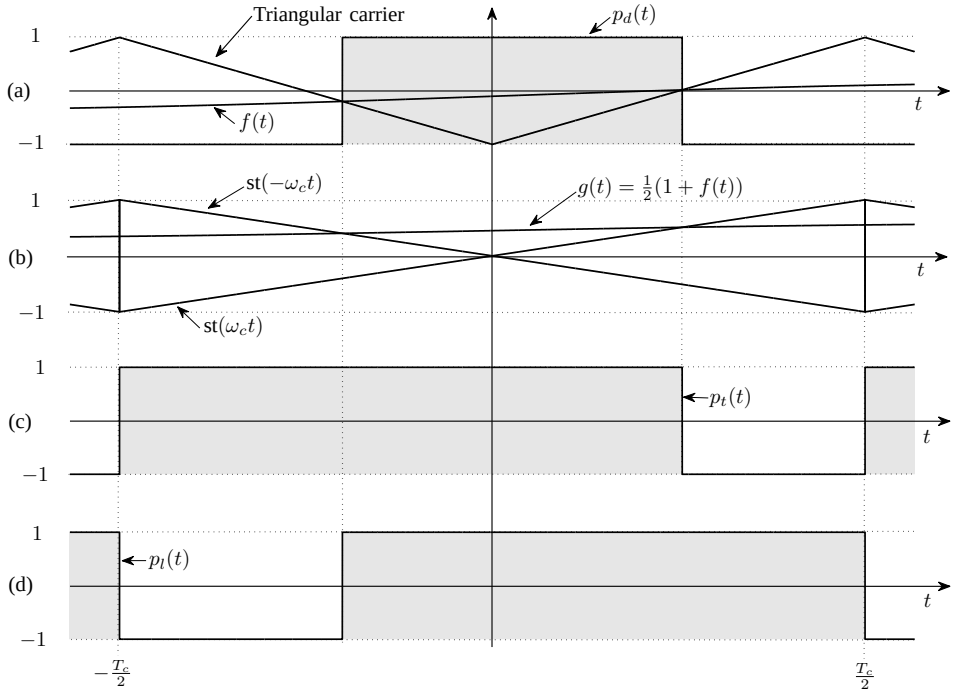

Fig. 2. Representing double-edge PWM by two single-edge modulators.

As shown in [19], this result is equivalent to a double Fourier series representation of the single-edge pulse train, but is more general in that it can treat non-periodic references. Also, the pulse train for a leading-edge modulator can be easily obtained from Eq. (3) by reversing the time of the carrier to yield:

$$p_l(t) = g(t) + st(\omega_c t) + \frac{j}{\pi} \sum_{\substack{m=-\infty \\ m\neq 0}}^{\infty} \frac{1}{m} e^{-jm(\omega_c t + \pi g(t))}. \tag{4}$$

III. The double-edge solution

It is well known that double-edge PWM can be represented by a leading edge and a trailing edge modulator [1]. Fig. 2(a) shows the double-edge PWM pulse train $p_d(t)$ generated by comparing the reference waveform $f(t)$ with a triangular carrier. Fig. 2(b) shows how the double-edge modulator can be represented by two single-edge modulators. The reference waveform $f(t)$ is level shifted by 1 and multiplied by $\frac{1}{2}$ to generate the new reference waveform $g(t) = \frac{1}{2}(1 + f(t))$ which serves as the reference signal for two single-edge modulators. The first, leading-edge modulator, compares $g(t)$ with the sawtooth carrier st$(-\omega_c t)$ to generate $p_l(t)$, while the second trailing-edge modulator compares $g(t)$ with the sawtooth carrier st$(\omega_c t)$ to generate $p_t(t)$. It is clear from the subsequent graphs that the original double-edge PWM pulse train $p_d(t)$ can be represented as $p_d(t) = p_l(t) + p_t(t) - 1$. Furthermore, since $g(t) = \frac{1}{2}(1 + f(t))$, it follows from equations (3) and (4) that

$$\begin{aligned} p_d(t) &= f(t) + \frac{j}{\pi} \sum_{\substack{m=-\infty \\ m\neq 0}}^{\infty} \frac{1}{m} \left\{ e^{jm(\omega_c t - \frac{\pi}{2}(1+f(t)))} + e^{-jm(\omega_c t + \frac{\pi}{2}(1+f(t)))} \right\} \\ &= f(t) + \frac{j}{\pi} \sum_{\substack{m=-\infty \\ m\neq 0}}^{\infty} \frac{1}{m} \left\{ e^{jm(\omega_c t - \frac{\pi}{2}(1+f(t)))} \right\} + \frac{j}{\pi} \sum_{\substack{m=-\infty \\ m\neq 0}}^{\infty} \frac{1}{m} \left\{ e^{-jm(\omega_c t + \frac{\pi}{2}(1+f(t)))} \right\}. \end{aligned}$$

This article has been accepted for publication in a future issue of this journal, but has not been fully edited. Content may change prior to final publication. Citation information: DOI 10.1109/TPEL.2014.2304677, IEEE Transactions on Power Electronics

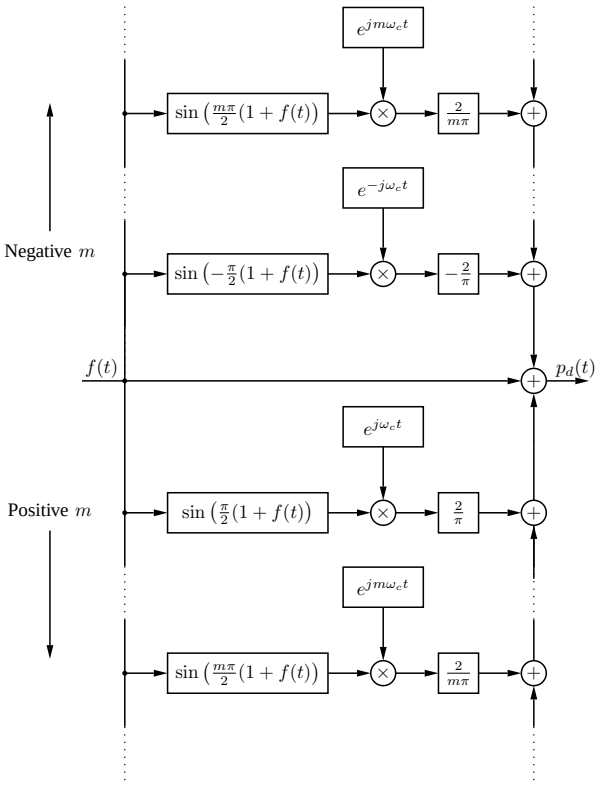

Fig. 3. Equivalent block diagram of the double-edge naturally-sampled pulse-width modulator.

Replacing m by $-m$ in the second summation results in

$$\begin{aligned} p_d(t) &= f(t) + \frac{j}{\pi} \sum_{\substack{m=-\infty \\ m\neq 0}}^{\infty} \frac{1}{m} \left\{ e^{jm(\omega_c t - \frac{\pi}{2}(1+f(t)))} - e^{jm(\omega_c t + \frac{\pi}{2}(1+f(t)))} \right\} \\ &= f(t) + \frac{j}{\pi} \sum_{\substack{m=-\infty \\ m\neq 0}}^{\infty} \frac{1}{m} e^{jm\omega_c t} \left\{ e^{-jm\frac{\pi}{2}(1+f(t))} - e^{jm\frac{\pi}{2}(1+f(t))} \right\} \quad (5) \\ &= f(t) + \frac{2}{\pi} \sum_{\substack{m=-\infty \\ m\neq 0}}^{\infty} \frac{1}{m} e^{jm\omega_c t} \sin\left(\frac{m\pi}{2}(1+f(t))\right). \quad (6) \end{aligned}$$

Fig. 3 shows the equivalent block diagram of the double-edge pulse-width modulator based on Eq. (6). Recall that multiplication by $e^{jm\omega_c t}$ in the time-domain corresponds to a frequency shift by $m\omega_c$ in the frequency domain. The block diagram thus shows that the pulse-width modulator is equivalent to a sequence of phase modulators, with each phase modulator producing a sideband of harmonics around an integer multiple $m\omega_c$ of the switching frequency. Each sideband is generated by the $\sin\left(\frac{m\pi}{2}(1+f(t))\right)$ non-linearity. The output of this non-linearity is multiplied by a factor $\frac{2}{m\pi}$. The PWM pulse train $p_d(t)$ also contains a copy of the original reference signal $f(t)$. Note that the sawtooth carrier, which was present in the expression for the PWM pulse train of single-edge modulation, cancels between the leading and trailing edge modulators and is not present in the expression for double-edge PWM.

Taking the Fourier transform of (6) results in an expression for the Fourier transform $P_d(\omega)$ of $p_d(t)$:

$$P_d(\omega) = F(\omega) + \sum_{\substack{m=-\infty \\ m\neq 0}}^{\infty} \int_{-\infty}^{\infty} \frac{2}{m\pi} \sin\left(\frac{m\pi}{2}(1+f(t))\right) e^{-j(\omega - m\omega_c)t}\, dt \quad (7)$$

This article has been accepted for publication in a future issue of this journal, but has not been fully edited. Content may change prior to final publication. Citation information: DOI 10.1109/TPEL.2014.2304677, IEEE Transactions on Power Electronics

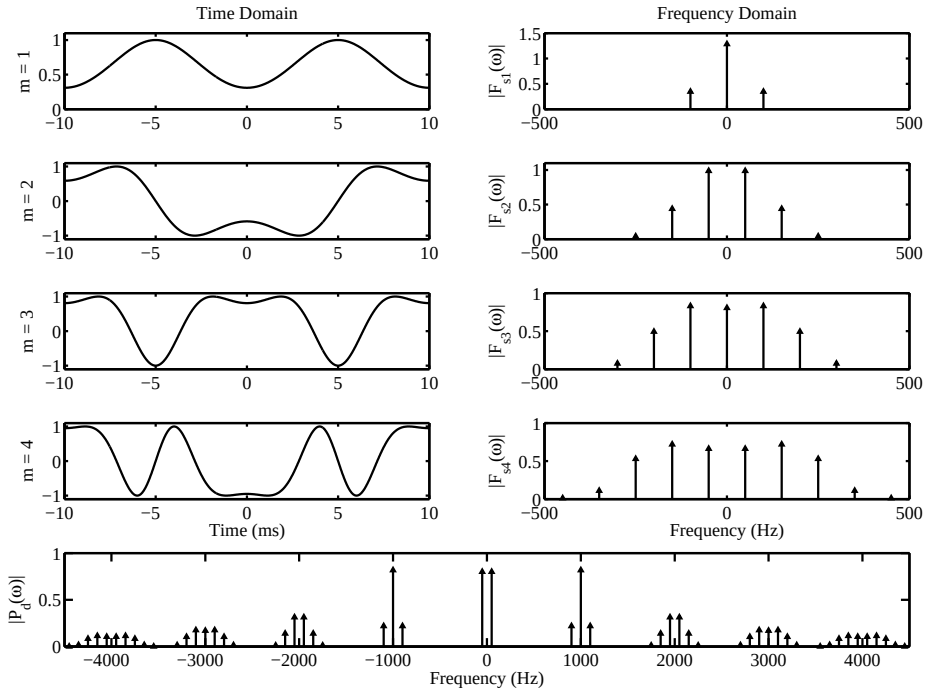

Fig. 4. Generating the sidebands for $f(t) = 0.8\cos(2\pi \times 50t)$ and a switching frequency of 1 kHz.

Fig. 4 illustrates the way in which the sidebands are generated by means of an example. The reference signal is $f(t) = 0.8\cos(2\pi \times 50t)$ and the switching frequency is 1 kHz. The smaller graphs show the output signals of the first four branches ($m = 1, 2, 3, 4$) of the block diagram of the pulse-width modulator shown in Fig. 3. The time-domain output signals are shown on the left and the Fourier transforms of the respective signals on the right. The Fourier transforms are multiplied by $\frac{2}{m\pi}$ and shifted to the right by $m\omega_c$ to form the sidebands of the PWM spectrum. The full PWM spectrum is shown in the bottom graph and also contains a copy of the original reference signal.

IV. Regular Sampling

In most digital implementations of PWM the reference signal is sampled and then held constant during each switching period or half of the switching period [20]. For symmetrical regular sampling, the reference $f(t)$ is sampled at either the positive or negative peak of the carrier and held constant for the entire switching period. For asymmetrical regular sampling the reference is sampled twice per switching period, at both peaks of the carrier. The sampling process produces a stepped reference signal which is phase delayed with respect to the original reference waveform $f(t)$. For symmetrical regular sampling this phase delay is half a switching period, while it is a quarter switching period for asymmetrical regular sampling. The phase delay can be compensated by advancing the reference signal. However, the same result can be obtained by advancing the sampling points of the reference rather than advancing the reference itself [9].

The approach followed in this paper is quite distinct from the double Fourier series approach which requires modification of the integration limits as an initial step [21], [22]. The regular sampling process is incorporated through multiplication by an impulse train, corresponding to the sampling instances, followed by a zero-order-hold filter. The interaction between the PWM non-linearity and the regular sampling process is studied and general equations for the harmonic spectra for both types of

This article has been accepted for publication in a future issue of this journal, but has not been fully edited. Content may change prior to final publication. Citation information: DOI 10.1109/TPEL.2014.2304677, IEEE Transactions on Power Electronics

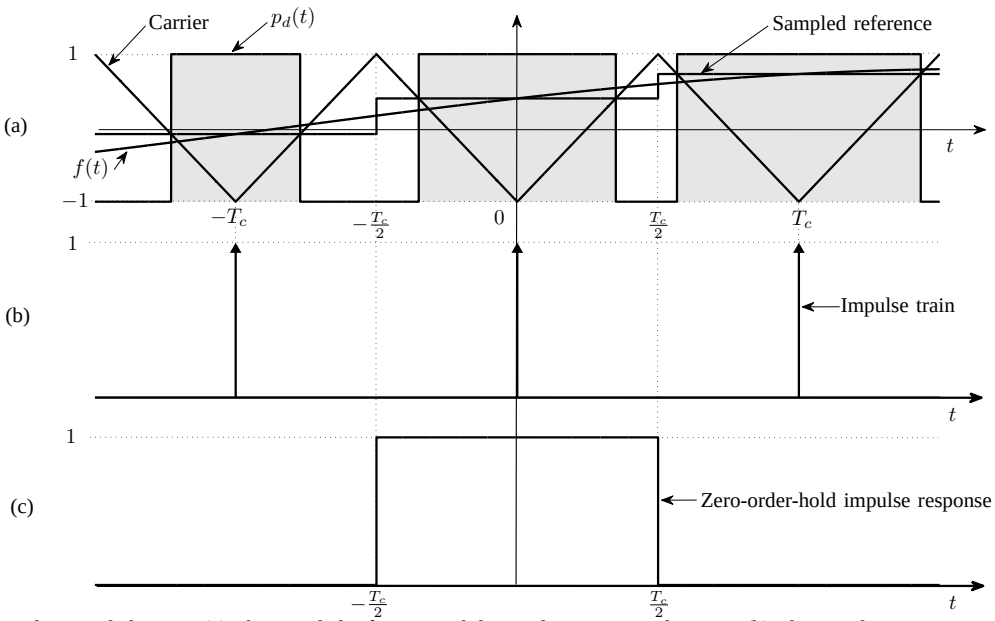

Fig. 5. Symmetrical regular sampled PWM. (a) The sampled reference and the resulting PWM pulse train. (b) The impulse train associated with the sampling instances. (c) The impulse response of the zero-order-hold filter.

regular sampling are developed. It is shown how the sampling process results in a frequency-domain duplication and filtering of the PWM sidebands. New sidebands are formed through the contributions of all branches of the equivalent model of the pulse-width modulator.

A. Symmetrical regular sampling

Fig. 5(a) illustrates the process of symmetrical regular sampling. The sampling points are phase-compensated as described above. It is well known from signal theory that the sample-and-hold process can be modeled as a multiplication by an impulse train followed by a zero-order hold filter [23]. These impulses are located at the sampling points as shown in Fig. 5(b) and the impulse response of the zero-order-hold filter (shown in Fig. 5(c)) represents the process of holding the sampled reference constant for a switching period.

In order to model the sample-and-hold process, first consider the impulse train with impulses located at the negative peaks of the triangular carrier as shown in Fig. 5(b). The Fourier series expansion of this impulse train is given by:

$$\mathrm{it}(t) = \frac{1}{T_c} \sum_{k=-\infty}^{\infty} e^{jk\omega_c t}$$

Furthermore, the transfer function of the zero-order-hold filter is given by:

$$\mathrm{ZOH}(\omega) = T_c \frac{\sin(\omega T_c/2)}{\omega T_c/2}$$

Fig. 6 shows three equivalent versions of the m'th branch of the symmetric regular sampled pulse-width modulator including the sample-and-hold block. In Fig. 6(a) the sample-and-hold block is placed between the input of the modulator and the nonlinear $\sin\left(\frac{m\pi}{2}(1+f(t))\right)$ block. Due to the nature of this nonlinearity, in particular the fact that it has no memory, the sample-and-hold register can be interchanged with the non-linear block as shown in Fig 6(b). In Fig. 6(c) the sample-and-hold block is replaced by the multiplication by the impulse train $\mathrm{it}(t)$ followed by the zero-order-hold filter.

This article has been accepted for publication in a future issue of this journal, but has not been fully edited. Content may change prior to final publication. Citation information: DOI 10.1109/TPEL.2014.2304677, IEEE Transactions on Power Electronics

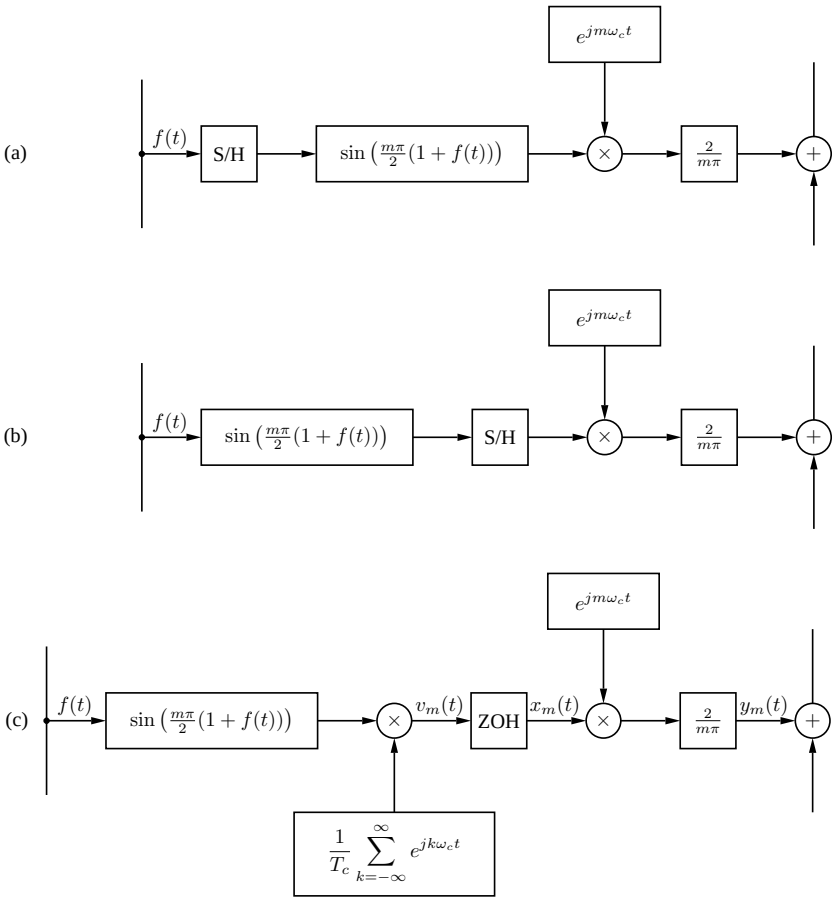

Fig. 6. Three equivalent versions of the m'th branch of symmetrical regular sampled PWM.

Define $F_{sm}(\omega)$ as the Fourier transform of the output of the m'th nonlinear $\sin\left(\frac{m\pi}{2}(1+f(t))\right)$ block, i.e.

$$\begin{aligned} F_{sm}(\omega) &:= \mathcal{F}\left\{\sin\left(\frac{m\pi}{2}(1+f(t))\right)\right\} \\ &= \int_{-\infty}^{\infty} \sin\left(\frac{m\pi}{2}(1+f(t))\right) e^{-j\omega t}\, dt \end{aligned}$$

The next step is to consider the Fourier transform $V_m(\omega)$ of $v_m(t)$. Since multiplication by $e^{jk\omega_c t}$ in the time domain corresponds to a frequency shift by $k\omega_c$ in the frequency domain it follows that

$$V_m(\omega) = \sum_{k=-\infty}^{\infty} F_{sm}(\omega - k\omega_c).$$

Passing $v_m(t)$ through the zero-order-hold filter results in the following expression for the Fourier transform $X_m(\omega)$ of $x_m(t)$:

$$X_m(\omega) = \frac{\sin(\omega T_c/2)}{\omega T_c/2} \sum_{k=-\infty}^{\infty} F_{sm}(\omega - k\omega_c)$$

Finally $x_m(t)$ is multiplied by $e^{jm\omega_c t}$ (again resulting in a frequency shift by $m\omega_c$) and then multiplied by $\frac{2}{m\pi}$ to produce the output signal $y_m(t)$ of the m'th modulator branch. The Fourier transform of $y_m(t)$ is given by:

$$Y_m(\omega) = \frac{2}{m\pi} \frac{\sin((\omega - m\omega_c)\frac{T_c}{2})}{(\omega - m\omega_c)\frac{T_c}{2}} \sum_{k=-\infty}^{\infty} F_{sm}(\omega - (k+m)\omega_c)$$

The final step in the analysis is to add the output signals of all the branches together. This summation should also contain a sampled-and-held copy of the original reference waveform. After some considerable mathematical manipulation an expression

This article has been accepted for publication in a future issue of this journal, but has not been fully edited. Content may change prior to final publication. Citation information: DOI 10.1109/TPEL.2014.2304677, IEEE Transactions on Power Electronics

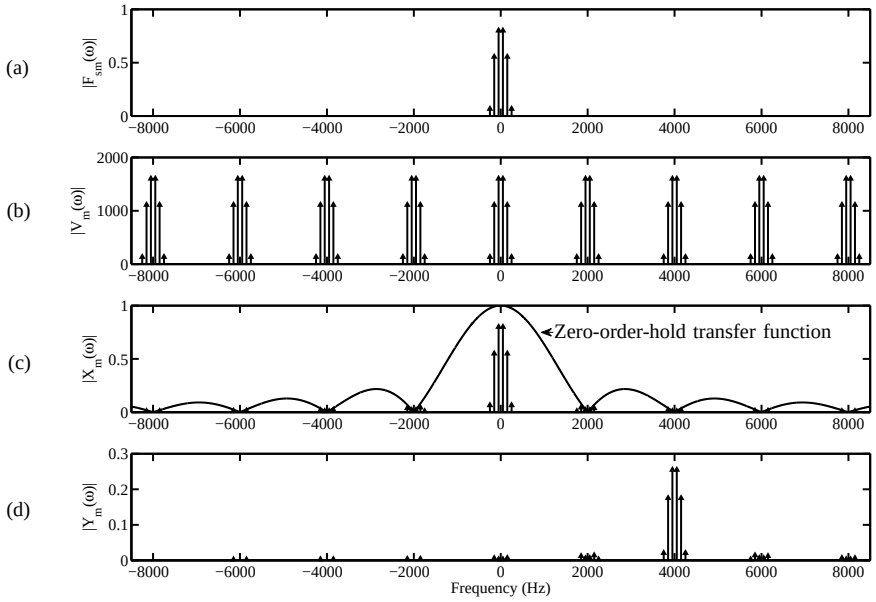

Fig. 7. Interaction of the pulse-width modulator and the sample-and-hold block for $m = 2$.

for the Fourier transform of the symmetrical regular sampled PWM pulse train $p_d(t)$ can be derived, i.e.

$$P_d(\omega) = \sum_{m=-\infty}^{\infty} \int_{-\infty}^{\infty} \frac{2\omega_c}{\pi\omega} \sin\left(\frac{\omega}{\omega_c}\left(\frac{\pi}{2}(1+f(t))\right)\right) e^{-j(\omega - m\omega_c)t}\, dt \tag{8}$$

It should be pointed out that Eq. (8) does not apply to the case where $\omega = 0$. The DC-component $P_d(0)$ consists only of the DC component of the sampled-and-held copy of the reference $f(t)$.

In order to illustrate the principles involved, Fig. 7 shows the frequency-domain sidebands generated by the branch for m=2 within Fig. 6. In this example $f(t) = 0.7\cos(2\pi \times 50t)$ and the switching frequency is 2 kHz. Fig. 7(a) shows the magnitude of the Fourier transform $F_{sm}(\omega)$ of the output of the PWM non-linearity. The sampler multiplies this signal by $\frac{1}{T_c}$ and generates images at integer multiples of the switching frequency as shown in Fig. 7(b). These images are filtered by the zero-order-hold filter as shown in Fig. 7(c). The zero-order-hold filter is a low-pass sinc filter with zeros located at all nonzero integer multiples of the switching frequency. Finally, multiplication by $e^{jm\omega_c t}$ shifts the whole spectrum to the right by $m\omega_c$ as shown in Fig. 7(d). The PWM pulse train is the sum of the output signals of all the different branches ($m = \pm 1, \pm 2, \ldots$) as well as a sampled-and-held copy of the original modulating waveform $f(t)$. New sidebands are formed when summing the contributions of all the branches. This model of the regular sampled pulse-width modulator clearly shows how baseband harmonics are generated. These are formed by the contributions of all the branches that, after frequency shifting, are situated around 0 Hz. Eliminating these baseband harmonics have been the subject of a number of papers in the field of digital class-d amplification [24]–[26].

B. Asymmetrical regular sampling

Fig. 8(a) illustrates the process of asymmetrical regular sampling. The sampling points are again phase-compensated as described in the previous section. For asymmetrical regular sampling the reference is sampled twice per switching period, at the two zero crossings of the carrier. The impulse train associated with the sampling points is shown in Fig. 8(b). The sampled reference is held constant for half a switching period. The impulse response of the associated zero-order-hold filter is shown in Fig. 8(c).

This article has been accepted for publication in a future issue of this journal, but has not been fully edited. Content may change prior to final publication. Citation information: DOI 10.1109/TPEL.2014.2304677, IEEE Transactions on Power Electronics

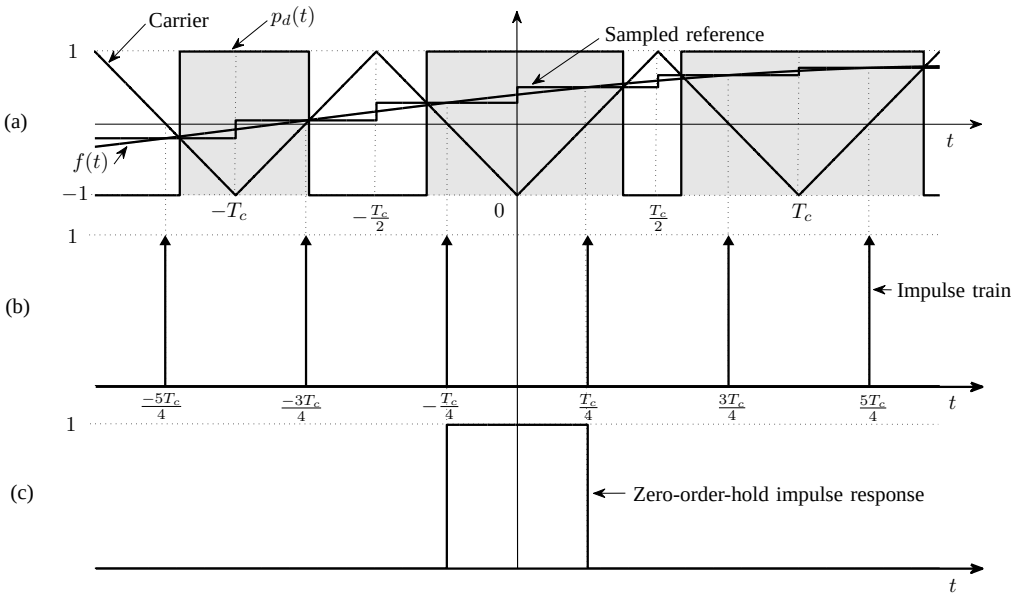

Fig. 8. Asymmetrical regular sampled PWM. (a) The sampled reference and the resulting PWM pulse train. (b) The impulse train associated with the sampling instances. (c) The impulse response of the zero-order-hold filter.

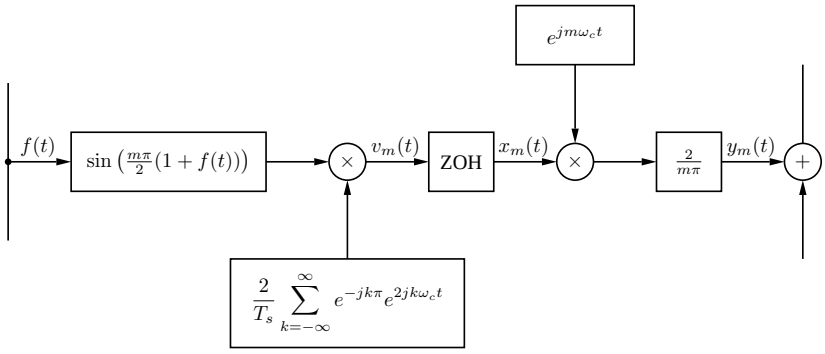

Fig. 9. The m'th branch of the asymmetrically regular sampled pulse-width modulator.

The Fourier series expansion of this impulse train shown in Fig. 8(b) is now given by:

$$\text{it}(t) = \frac{2}{T_c}\sum_{k=-\infty}^{\infty} e^{-jk\pi}e^{2jk\omega_c t}$$

Furthermore, the transfer function of the zero-order-hold filter of Fig. 8(c) is given by:

$$\text{ZOH}(\omega) = \frac{T_c}{2}\frac{\sin(\omega T_c/4)}{\omega T_c/4}$$

In this case

$$V_m(\omega) = \frac{2}{T_c}\sum_{k=-\infty}^{\infty} e^{-jk\pi}F_{sm}(\omega - 2k\omega_c),$$

$$X_m(\omega) = \frac{\sin(\omega T_c/4)}{\omega T_c/4}\sum_{k=-\infty}^{\infty} e^{-jk\pi}F_{sm}(\omega - 2k\omega_c)$$

and

$$Y_m(\omega) = \frac{2}{m\pi}\frac{\sin((\omega - m\omega_c)\frac{T_c}{4})}{(\omega - m\omega_c)\frac{T_c}{4}}\sum_{k=-\infty}^{\infty} e^{-jk\pi}F_{sm}(\omega - (2k+m)\omega_c).$$

This article has been accepted for publication in a future issue of this journal, but has not been fully edited. Content may change prior to final publication. Citation information: DOI 10.1109/TPEL.2014.2304677, IEEE Transactions on Power Electronics

TABLE I

THE VALUES OF $\alpha(\omega)$, $\beta(\omega)$ AND $\gamma(\omega)$ FOR DIFFERENT SAMPLING METHODS.

Sampling method	$\alpha(\omega)$	$\beta(\omega)$	$\gamma(\omega)$
Naturally sampled	$\frac{2}{m\pi}$	$\frac{m\pi}{2}$	$\frac{m\pi}{2}$
Symmetric regular sampled	$\frac{2}{\pi}\frac{\omega_c}{\omega}$	$\frac{\pi}{2}\frac{\omega}{\omega_c}$	$\frac{\pi}{2}\frac{\omega}{\omega_c}$
Asymmetric regular sampled	$\frac{2}{\pi}\frac{\omega_c}{\omega}$	$\frac{\pi}{2}m$	$\frac{\pi}{2}\frac{\omega}{\omega_c}$

By again summing the contributions of all the branches together it can be shown that:

$$P_d(\omega) = \sum_{m=-\infty}^{\infty} \int_{-\infty}^{\infty} \frac{2\omega_c}{\pi\omega} \sin\left(\frac{\pi}{2}\left(m + \frac{\omega}{\omega_c} f(t)\right)\right) e^{-j(\omega - m\omega_c)t} dt \tag{9}$$

Equation (9) does not apply to the case where $\omega = 0$. As for symmetric regular sampling $P_d(0)$ consist only of the DC component of the sampled-and-held copy of the reference $f(t)$. However, the reference is now sampled at twice the switching frequency.

To summarize , the Fourier transform $P_d(\omega)$ of the PWM pulse train is given by the following equations:
For naturally sampled PWM (from Eq. (7)):

$$P_d(\omega) = F(\omega) + \sum_{\substack{m=-\infty \\ m\neq 0}}^{\infty} \int_{-\infty}^{\infty} \frac{2}{m\pi} \sin\left(\frac{m\pi}{2}(1 + f(t))\right) e^{-j(\omega - m\omega_c)t}\, dt$$

For symmetric regular sampled PWM (from Eq. (8)):

$$P_d(\omega) = \sum_{m=-\infty}^{\infty} \int_{-\infty}^{\infty} \frac{2\omega_c}{\pi\omega} \sin\left(\frac{\omega}{\omega_c}\left(\frac{\pi}{2}(1 + f(t))\right)\right) e^{-j(\omega - m\omega_c)t}\, dt$$

For asymmetric regular sampled PWM (from Eq. (9)):

$$P_d(\omega) = \sum_{m=-\infty}^{\infty} \int_{-\infty}^{\infty} \frac{2\omega_c}{\pi\omega} \sin\left(\frac{\pi}{2}\left(m + \frac{\omega}{\omega_c} f(t)\right)\right) e^{-j(\omega - m\omega_c)t} dt$$

The integral describing the m'th sideband in each of the above equations is of the general form:

$$S_m(\omega) = \int_{-\infty}^{\infty} \alpha(\omega) \sin(\beta(\omega) + \gamma(\omega) f(t)) e^{-j(\omega - m\omega_c)t}\, dt \tag{10}$$

The values of $\alpha(\omega)$, $\beta(\omega)$ and $\gamma(\omega)$ for the different sampling methods are listed in Table I. It is easy to see from Eq. (10) that delaying the reference by t_0 in the time domain implies that $S_m(\omega)$ must be multiplied by $e^{-j(\omega - m\omega_c)t_0}$ in the frequency domain. This observation will be used later when calculating the spectra of the line-to-line voltages of three-phase converters.

V. PERIODIC REFERENCES

The equations derived thus far apply to periodic as well as aperiodic references. However, in most practical applications of PWM a periodic reference signal is used. For this reason assume that $f(t)$ is periodic with period T_0 and frequency $\omega_0 = \frac{2\pi}{T_0}$. In this case:

$$\begin{aligned} S_m(\omega) &= \int_{-\infty}^{\infty} \alpha(\omega) \sin\left(\beta(\omega) + \gamma(\omega) f(t)\right) e^{-j(\omega - m\omega_c)t}\, dt \\ &= \int_{-\infty}^{\infty} \frac{\alpha(\omega)}{2j} \left\{ e^{j\beta(\omega)} e^{j\gamma(\omega) f(t)} - e^{-j\beta(\omega)} e^{-j\gamma(\omega) f(t)} \right\} e^{-j(\omega - m\omega_c)t}\, dt \end{aligned} \tag{11}$$

This article has been accepted for publication in a future issue of this journal, but has not been fully edited. Content may change prior to final publication. Citation information: DOI 10.1109/TPEL.2014.2304677, IEEE Transactions on Power Electronics

For every fixed value of ω and fixed value of m, the function $e^{j\gamma(\omega)f(t)}$ is a periodic function of time and thus has an exponential Fourier series expansion of the form

$$e^{j\gamma(\omega)f(t)} = \sum_{n=-\infty}^{\infty} C_{mn}(\omega)e^{jn\omega_0 t},$$

where

$$C_{mn}(\omega) = \frac{1}{T_0}\int_{t_0}^{t_0+T_0} e^{j\gamma(\omega)f(t)}e^{-jn\omega_0 t}\,dt. \tag{12}$$

Note that the Fourier coefficients $C_{mn}(\omega)$ are functions of ω. Furthermore, the function $e^{-j\gamma(\omega)f(t)}$ also has an exponential Fourier series expansion of the form:

$$e^{-j\gamma(\omega)f(t)} = \sum_{n=-\infty}^{\infty} D_{mn}(\omega)e^{jn\omega_0 t},$$

where

$$\begin{aligned} D_{mn}(\omega) &= \frac{1}{T_0}\int_{t_0}^{t_0+T_0} e^{-j\gamma(\omega)f(t)}e^{-jn\omega_0 t}\,dt \\ &= \overline{C}_{m(-n)}(\omega). \end{aligned}$$

Hence, according to Eq. (11):

$$\begin{aligned} S_m(\omega) &= \int_{-\infty}^{\infty}\frac{\alpha(\omega)}{2j}\left\{e^{j\beta(\omega)}\sum_{n=-\infty}^{\infty}C_{mn}(\omega)e^{jn\omega_0 t} - e^{-j\beta(\omega)}\sum_{n=-\infty}^{\infty}\overline{C}_{m(-n)}(\omega)e^{-jn\omega_0 t}\right\}e^{-j(\omega-m\omega_c)t}\,dt \\ &= \pi\frac{\alpha(\omega)}{j}\left\{e^{j\beta(\omega)}\sum_{n=-\infty}^{\infty}C_{mn}(\omega)\delta(\omega-n\omega_0-m\omega_c) - e^{-j\beta(\omega)}\sum_{n=-\infty}^{\infty}\overline{C}_{m(-n)}(\omega)\delta(\omega-n\omega_0-m\omega_c)\right\} \end{aligned}$$

A well-known property of the Dirac-delta distribution $\delta(x)$ is the fact that $f(x)\delta(x-y) = f(y)\delta(x-y)$ [27]. Hence, since the impulses occur at $\omega = n\omega_0 + m\omega_c$ in the frequency domain, $S_m(\omega)$ can be rewritten as:

$$\begin{aligned} S_m(\omega) = \pi\sum_{n=-\infty}^{\infty}\frac{\alpha(n\omega_0+m\omega_c)}{j}&\Big\{C_{mn}(n\omega_0+m\omega_c)e^{j\beta(n\omega_0+m\omega_c)} \\ &-\overline{C}_{m(-n)}(n\omega_0+m\omega_c)e^{-j\beta(n\omega_0+m\omega_c)}\Big\}\delta(\omega-n\omega_0-m\omega_c) \end{aligned} \tag{13}$$

It is interesting to note that according to Eq. (13) the spectrum can be represented by a sequence of impulses even though the time-domain PWM pulse train is not necessarily periodic.

VI. Sinusoidal modulation

For sinusoidal modulation the reference function $f(t)$ is of the form

$$f(t) = M\cos(\omega_0 t),$$

where M is the modulation index. The first step in determining an expression for the PWM spectrum is to determine the Fourier coefficients $C_{mn}(\omega)$ as defined in Eq. (12). These coefficients can easily be identified from the Jacobi-Anger expansion [28] according to which

$$e^{j\gamma(\omega)M\cos(\omega_0 t)} = \sum_{n=-\infty}^{\infty} j^n J_n\left(\gamma(\omega)M\right)e^{jn\omega_0 t}.$$

Hence

$$C_{mn}(\omega) = j^n J_n\left(\gamma(\omega)M\right).$$

This article has been accepted for publication in a future issue of this journal, but has not been fully edited. Content may change prior to final publication. Citation information: DOI 10.1109/TPEL.2014.2304677, IEEE Transactions on Power Electronics

TABLE II

SPECTRA OF SINUSOIDAL PWM

Naturally sampled
$P_d(\omega) = \pi M\left(\delta(\omega-\omega_0)+\delta(\omega+\omega_0)\right) + \sum_{\substack{m=-\infty \\ m\neq 0}}^{\infty}\sum_{n=-\infty}^{\infty} \frac{4}{m} J_n\left(m\frac{\pi}{2}M\right)\sin\left((m+n)\frac{\pi}{2}\right)\delta(\omega-n\omega_0-m\omega_c)$
Symmetric regular sampled
$P_d(\omega) = \sum_{m=-\infty}^{\infty}\sum_{n=-\infty}^{\infty} 4\frac{1}{n\frac{\omega_0}{\omega_c}+m} J_n\left(\frac{\pi}{2}M\left(n\frac{\omega_0}{\omega_c}+m\right)\right)\sin\left(\left(n\frac{\omega_0}{\omega_c}+m+n\right)\frac{\pi}{2}\right)\delta(\omega-n\omega_0-m\omega_c)$
Asymmetric regular sampled
$P_d(\omega) = \sum_{m=-\infty}^{\infty}\sum_{n=-\infty}^{\infty} 4\frac{1}{n\frac{\omega_0}{\omega_c}+m} J_n\left(\frac{\pi}{2}M\left(n\frac{\omega_0}{\omega_c}+m\right)\right)\sin\left((m+n)\frac{\pi}{2}\right)\delta(\omega-n\omega_0-m\omega_c)$

Substituting this value of $C_{mn}(\omega)$ into Eq. (13) results in:

$$\begin{aligned} S_m(\omega) &= \pi\sum_{n=-\infty}^{\infty}\frac{\alpha(n\omega_0+m\omega_c)}{j}\Big\{j^n J_n\left(\gamma(n\omega_0+m\omega_c)M\right)e^{j\beta(n\omega_0+m\omega_c)} \\ &\qquad -(-j^{-n})J_{-n}\left(\gamma(n\omega_0+m\omega_c)M\right)e^{-j\beta(n\omega_0+m\omega_c)}\Big\}\delta(\omega-n\omega_0-m\omega_c) \\ &= 2\pi\sum_{n=-\infty}^{\infty}\alpha(n\omega_0+m\omega_c)J_n\left(\gamma(n\omega_0+m\omega_c)M\right)\sin\left(\beta(n\omega_0+m\omega_c)+n\frac{\pi}{2}\right)\delta(\omega-n\omega_0-m\omega_c) \end{aligned}$$

The next step is simply to select the value of $\alpha(\omega)$, $\beta(\omega)$ and $\gamma(\omega)$ for the particular sampling method from Table I. The resulting equations of the spectra of sinusoidal PWM for the three sampling methods are summarized in Table II.

The equations in Table II express the PWM spectra in terms of the Fourier transform. By making use of the fact that in all three cases the Fourier transform is real, these equations can easily be seen to be equivalent to equations (3.39), (3.78) and (3.98) of [9], which represent the spectra in terms of a double Fourier series.

VII. TIME DOMAIN ADDITION AND FREQUENCY DOMAIN CONVOLUTION

A fundamental question that arises is what happens to the PWM spectrum if the reference waveform consists of a sum of different time-domain waveforms. This question has been studied by other researchers when the modulating waveform contains a fundamental and a number of harmonic components [8], [29], [30]. The resulting equations are usually quite complex.

This paper follows a more fundamental approach to the question of time-domain addition of reference waveforms. Having identified the underlying non-linearity that generates the PWM sidebands, it is shown that addition of reference waveforms in the time domain results in a double convolution of the respective PWM sidebands in the frequency domain. It is not required that the superimposed reference waveforms are sinusoidal or harmonics of the fundamental.

Assume that $f(t) = g(t) + h(t)$ and that $g(t)$ and $h(t)$ are both periodic with period $\frac{2\pi}{\omega_0}$. Let $G_{mn}(\omega)$ and $H_{mn}(\omega)$ denote the exponential Fourier coefficients of $e^{j\gamma(\omega)g(t)}$ and $e^{j\gamma(\omega)h(t)}$, respectively (as defined by Eq. (12)). That is:

$$e^{j\gamma(\omega)g(t)} = \sum_{n=-\infty}^{\infty} G_{mn}(\omega)e^{jn\omega_0 t}$$

and

$$e^{j\gamma(\omega)h(t)} = \sum_{n=-\infty}^{\infty} H_{mn}(\omega)e^{jn\omega_0 t}.$$

This article has been accepted for publication in a future issue of this journal, but has not been fully edited. Content may change prior to final publication. Citation information: DOI 10.1109/TPEL.2014.2304677, IEEE Transactions on Power Electronics

It is well known that the multiplication of two exponential Fourier series results in the convolution of the Fourier coefficients [31], theorem 15.22. Hence

$$e^{j\gamma(\omega)g(t)}e^{j\gamma(\omega)h(t)} = \sum_{n=-\infty}^{\infty} P_{mn}(\omega)e^{jn\omega_0 t},$$

where

$$P_{mn}(\omega) = \sum_{k=-\infty}^{\infty} G_{m(n-k)}(\omega)H_{mk}(\omega).$$

According to Eq. (13) this means that the Fourier transform of the PWM sidebands of $f(t)$ can be written as:

$$\begin{aligned} S_m(\omega) &= \pi \sum_{n=-\infty}^{\infty} \frac{\alpha(n\omega_0 + m\omega_c)}{j} \Big\{ P_{mn}(n\omega_0 + m\omega_c)e^{j\beta(n\omega_0+m\omega_c)} \\ &\qquad -\overline{P}_{m(-n)}(n\omega_0 + m\omega_c)e^{-j\beta(n\omega_0+m\omega_c)} \Big\} \delta(\omega - n\omega_0 - m\omega_c) \end{aligned} \tag{14}$$

In [19] a similar result was derived for a single-edge naturally sampled modulator. For the single-edge modulator addition of reference signals in the time domain resulted in a standard convolution of the sidebands in the frequency domain. Equation (14) shows that for the double-edge modulator addition in the time domain results in a double convolution of sidebands in the frequency domain. This can be interpreted as one convolution process associated with each of the single-edge modulators that form the double-edge modulator as illustrated in Fig. 2.

By repeatedly applying Eq. (14) the PWM spectrum can be calculated if the reference waveform consists of a sum of any number of periodic waveforms. In the next two sections it will be shown that this convolution theorem is a powerful tool which significantly simplifies the calculation of the PWM spectra for third harmonic injection and space-vector modulation PWM.

VIII. Complex References

A. Third harmonic injection

It is well known that the maximum line-to-line output voltage of a three-phase inverter can be increased by including a common-mode third-order harmonic in the PWM reference waveform [32]. Since this third-order harmonic cancels between the phases, the line-to-line voltages remain sinusoidal. As a result the modulation index M can be increased beyond 1 without driving the pulse-width modulator into over modulation. In [9] section 5.3.1 it was shown that the optimal amplitude of the third harmonic component is equal to $-\frac{M}{6}$ which means that M can now be increased to 1.15.

In order to derive an expression for the PWM spectrum with third harmonic injection let

$$g(t) = M\cos(\omega_0 t) \quad \text{and} \quad h(t) = M_3\cos(3\omega_0 t),$$

where $M_3 = -\frac{M}{6}$. According to the Jacobi-Anger expansion

$$G_{mn}(\omega) = j^n J_n\left(\gamma(\omega)M\right) \tag{15}$$

and

$$H_{mn}(\omega) = \begin{cases} j^{\frac{n}{3}} J_{\frac{n}{3}}\left(\gamma(\omega)M_3\right) & \text{if n is an integer multiple of 3} \\ 0 & \text{otherwise} \end{cases} \tag{16}$$

Hence

$$\begin{aligned} P_{mn}(\omega) &= \sum_{k=-\infty}^{\infty} G_{m(n-k)}(\omega)H_{mk}(\omega) \\ &= \sum_{\substack{k=-\infty \\ k\in 3\mathbb{Z}}}^{\infty} J_{(n-k)}\left(\gamma(\omega)M\right) j^{\frac{k}{3}} J_{\frac{k}{3}}\left(\gamma(\omega)M_3\right) \end{aligned}$$

This article has been accepted for publication in a future issue of this journal, but has not been fully edited. Content may change prior to final publication. Citation information: DOI 10.1109/TPEL.2014.2304677, IEEE Transactions on Power Electronics

TABLE III

THEORETICAL SPECTRA OF THIRD HARMONIC INJECTION PWM

Naturally sampled

$$P_d(\omega) = \pi M\left(\delta(\omega-\omega_0)+\delta(\omega+\omega_0)\right) + \pi M_3\left(\delta(\omega-3\omega_0)+\delta(\omega+3\omega_0)\right)$$
$$+\sum_{\substack{m=-\infty\\ m\neq 0}}^{\infty}\sum_{n=-\infty}^{\infty}\frac{2}{mj}\left\{\sum_{\substack{k=-\infty\\ k\in 3\mathbb{Z}}}^{\infty} J_{\frac{k}{3}}\left(\frac{m\pi}{2}M_3\right)\left\{j^{(n-k)}J_{(n-k)}\left(\frac{m\pi}{2}M\right)j^{\frac{k}{3}}e^{j\frac{m\pi}{2}} - j^{(n+k)}J_{-(n+k)}\left(\frac{m\pi}{2}M\right)(-j)^{\frac{k}{3}}e^{-j\frac{m\pi}{2})}\right\}\right\}\delta(\omega-n\omega_0-m\omega_c)$$

Symmetric regular sampled

$$P_d(\omega) = \sum_{m=-\infty}^{\infty}\sum_{n=-\infty}^{\infty}\frac{2}{j\left(n\frac{\omega_0}{\omega_c}+m\right)}\left\{\sum_{\substack{k=-\infty\\ k\in 3\mathbb{Z}}}^{\infty} J_{\frac{k}{3}}\left(\frac{\pi}{2}\left(n\frac{\omega_0}{\omega_c}+m\right)M_3\right)\left\{j^{(n-k)}J_{(n-k)}\left(\frac{\pi}{2}\left(n\frac{\omega_0}{\omega_c}+m\right)M\right)j^{\frac{k}{3}}e^{j\frac{\pi}{2}\left(n\frac{\omega_0}{\omega_c}+m\right)}\right.\right.$$
$$\left.\left. -j^{(n+k)}J_{-(n+k)}\left(\frac{\pi}{2}\left(n\frac{\omega_0}{\omega_c}+m\right)M\right)(-j)^{\frac{k}{3}}e^{-j\frac{\pi}{2}\left(n\frac{\omega_0}{\omega_c}+m\right)}\right\}\right\}\delta(\omega-n\omega_0-m\omega_c)$$

Asymmetric regular sampled

$$P_d(\omega) = \sum_{m=-\infty}^{\infty}\sum_{n=-\infty}^{\infty}\frac{2}{j\left(n\frac{\omega_0}{\omega_c}+m\right)}\left\{\sum_{\substack{k=-\infty\\ k\in 3\mathbb{Z}}}^{\infty} J_{\frac{k}{3}}\left(\frac{\pi}{2}\left(n\frac{\omega_0}{\omega_c}+m\right)M_3\right)\left\{j^{(n-k)}J_{(n-k)}\left(\frac{\pi}{2}\left(n\frac{\omega_0}{\omega_c}+m\right)M\right)j^{\frac{k}{3}}e^{j\frac{\pi}{2}m}\right.\right.$$
$$\left.\left. -j^{(n+k)}J_{-(n+k)}\left(\frac{\pi}{2}\left(n\frac{\omega_0}{\omega_c}+m\right)M\right)(-j)^{\frac{k}{3}}e^{-j\frac{\pi}{2}m}\right\}\right\}\delta(\omega-n\omega_0-m\omega_c)$$

Note that the sum is taken over all integer multiples of 3.

According to the convolution theorem, Eq. (14):

$$\begin{aligned} S_m(\omega) &= \pi\sum_{n=-\infty}^{\infty}\frac{\alpha(n\omega_0+m\omega_c)}{j}\left\{P_{mn}(n\omega_0+m\omega_c)e^{j\beta(n\omega_0+m\omega_c)}\right. \\ &\qquad \left. -\overline{P}_{m(-n)}(n\omega_0+m\omega_c)e^{-j\beta(n\omega_0+m\omega_c)}\right\}\delta(\omega-n\omega_0-m\omega_c) \\ &= \pi\sum_{n=-\infty}^{\infty}\frac{\alpha(n\omega_0+m\omega_c)}{j}\left\{\sum_{\substack{k=-\infty\\ k\in 3\mathbb{Z}}}^{\infty} J_{\frac{k}{3}}\left(\gamma(n\omega_0+m\omega_c)M_3\right)\left\{j^{(n-k)}J_{(n-k)}\left(\gamma(n\omega_0+m\omega_c)M\right)j^{\frac{k}{3}}e^{j\beta(n\omega_0+m\omega_c)}\right.\right. \\ &\qquad \left.\left. -j^{(n+k)}J_{-(n+k)}\left(\gamma(n\omega_0+m\omega_c)M\right)(-j)^{\frac{k}{3}}e^{-j\beta(n\omega_0+m\omega_c)}\right\}\right\}\delta(\omega-n\omega_0-m\omega_c) \end{aligned}$$

The next step is again to simply select the value of $\alpha(\omega)$, $\beta(\omega)$ and $\gamma(\omega)$ for the particular sampling method from Table I. The resulting equations for the three sampling methods provide new analytic solution for the spectra of third harmonic injection PWM and are summarized in Table III. As pointed out in [9] the analytic equations for the spectra of complex modulation strategies can only be represented in the form of series expansions. It should again be noted that the equations for symmetric and asymmetric regular sampling in Table III does not apply to the DC-component ($\omega = 0$). As mentioned previously the DC-component consists of the sampled and held copy of the reference. Any combination of m and n that results in $n\omega_0 + m\omega_c = 0$ should again be disregarded.

Fig. 10 illustrates how the PWM sidebands are generated through the convolution process under the conditions $M = 0.8$ and $\frac{f_c}{f_0} = 40$ for naturally sampled third order harmonic injection PWM. Figures 10(a) and (b) show the magnitudes of $G_{mn}(\omega)$ and $H_{mn}(\omega)$, respectively. These were calculated by means of equations (15) and (16). Fig. 10(c) shows the total harmonic spectrum for third harmonic PWM. For comparison Fig. 10(d) shows the harmonic sidebands for sinusoidal PWM under the

This article has been accepted for publication in a future issue of this journal, but has not been fully edited. Content may change prior to final publication. Citation information: DOI 10.1109/TPEL.2014.2304677, IEEE Transactions on Power Electronics

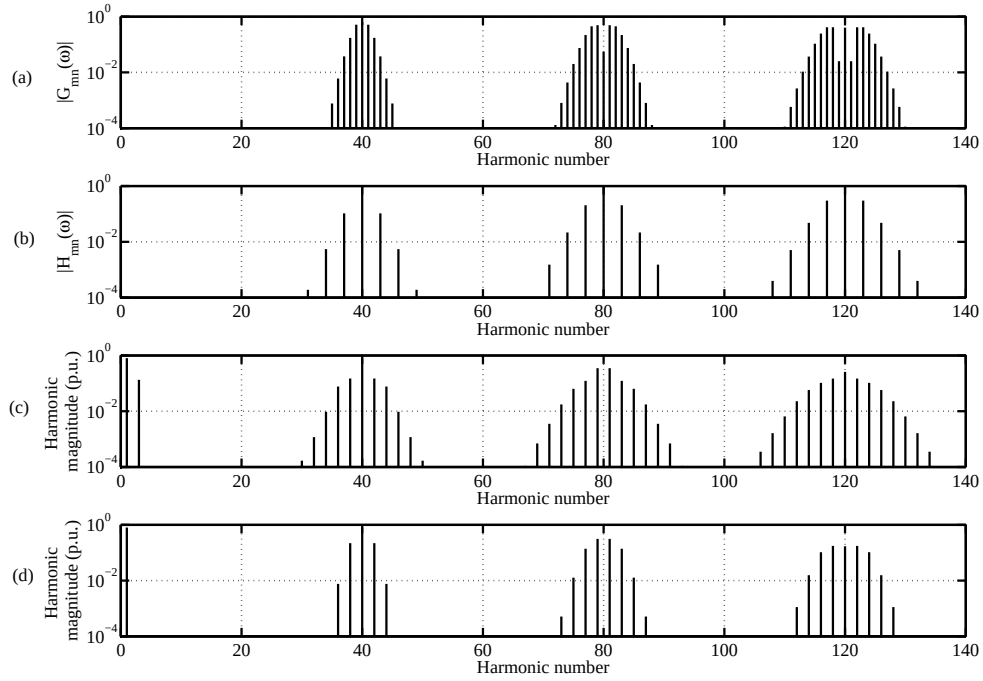

Fig. 10. Generation of the naturally sampled third harmonic injection sidebands for $M = 0.8$ and $\frac{f_c}{f_0} = 40$. (a) Absolute value of $G_{mn}(\omega)$ (b) Absolute value of $H_{mn}(\omega)$ (c) Harmonic spectrum of third harmonic injection PWM (d) Harmonic spectrum of sinusoidal PWM.

same conditions. It is evident how convolution between the respective sidebands of figures 10(a) and (b) results in a widening and flattening of the sidebands in Fig. 10(c) compared to sinusoidal PWM. This rearrangement of the sidebands results in a reduction of the Weighted Total Harmonic Distortion (WTHD) [9] of the line-to-line voltages from 1.26% for sinusoidal modulation to 1.14% for third harmonic injection PWM. In the process of applying Eq. (14) all sideband harmonics for which n is even cancel out. Fig. 10(c) also shows the fundamental sinusoidal component as well as the injected third order harmonic. This harmonic as well as all the sideband harmonics for which n is an integer multiple of three cancel out when calculating the line-to-line voltages.

B. Space-vector modulation

Space vector modulation (SVM) was introduced in the 1980's and has since become a standard for three-phase voltage source inverters. The relationship between space-vector modulation and carrier-based PWM has been known for a number of years [33]–[38]. The method presented in [9] for deriving analytic equations for the harmonics of SVM requires considerable algebraic manipulation. In this paper it is shown how alternative analytic equations can be derived in a few steps by using the convolution theorem.

In [9], section 6.2, it was shown that the modulating waveform for space vector modulation $f(t)$ consists of two components, i.e. $f(t) = g(t) + h(t)$, where $g(t) = M\cos(\omega_0 t)$ and $h(t)$ is a triangular waveform, defined by

$$h(t) = \begin{cases} -A\left(\frac{4}{T_1}t + 1\right) & \text{if } -\frac{T_1}{3} \le t \le 0 \\ A\left(\frac{4}{T_1}t - 1\right) & \text{if } 0 \le t \le \frac{T_1}{3} \end{cases}$$

over the interval $[-\frac{T_1}{3}, \frac{T_1}{3}]$ and extended periodically for all other values of time. Note that $A = \frac{M}{4}$, $T_1 = \frac{T_0}{3}$ and $\omega_1 = 3\omega_0$.

This article has been accepted for publication in a future issue of this journal, but has not been fully edited. Content may change prior to final publication. Citation information: DOI 10.1109/TPEL.2014.2304677, IEEE Transactions on Power Electronics

TABLE IV

COEFFICIENTS FOR SVM

Naturally sampled SVM	
$G_{mn}(\omega) = j^n J_n\left(m\frac{\pi}{2}M\right)$	$H_{mn}(\omega) = \begin{cases} \frac{e^{-jm\frac{\pi}{2}A}}{j}\left\{\frac{mA\left(e^{j(mA+n)\pi}-1\right)}{\pi(m^2A^2-n^2)}\right\} & \text{if } m^2A^2-n^2 \neq 0 \\ \frac{e^{-jm\frac{\pi}{2}A}}{2} & \text{if } m^2A^2-n^2=0 \text{ and } n\neq 0 \\ 1 & \text{if } mA=n=0 \end{cases}$
Symmetric regular or asymmetric regular sampled SVM	
$G_{mn}(\omega) = j^n J_n\left(\frac{\pi}{2}\frac{\omega}{\omega_c}M\right)$	$H_{mn}(\omega) = \begin{cases} \frac{e^{-j\frac{\pi}{2}\frac{\omega}{\omega_c}A}}{j\pi}\left\{\frac{A\frac{\omega}{\omega_c}\left(e^{-j\left(\pi\frac{\omega}{\omega_c}A+n\pi\right)}-1\right)}{A^2\left(\frac{\omega}{\omega_c}\right)^2-n^2}\right\} & \text{if } A^2\left(\frac{\omega}{\omega_c}\right)^2-n^2\neq 0 \\ \frac{e^{-j\frac{\pi}{2}\frac{\omega}{\omega_c}A}}{2} & \text{if } A^2\left(\frac{\omega}{\omega_c}\right)^2-n^2=0 \text{ and } n\neq 0 \\ 1 & \text{if } A=n=0 \end{cases}$

In order to apply the convolution theorem, Eq. (14), the exponential Fourier-series expansions of $e^{j\gamma(\omega)g(t)}$ and $e^{j\gamma(\omega)h(t)}$ must first be calculated. The Fourier series expansion of $e^{j\gamma(\omega)g(t)}$ again follow directly from the Jacobi-Anger expansion, i.e.

$$e^{j\gamma(\omega)g(t)} = \sum_{n=-\infty}^{\infty} G_{mn}(\omega)e^{jn\omega_0 t} \quad \text{where} \quad G_{mn}(\omega) = j^n J_n\left(\gamma(\omega)M\right).$$

On the other hand the Fourier coefficients of $e^{j\gamma(\omega)h(t)}$ can be calculated by solving the integrals describing the Fourier coefficients. Using elementary techniques it is easy to show that

$$e^{j\gamma(\omega)h(t)} = \sum_{n=-\infty}^{\infty} H_{mn}(\omega)e^{jn\omega_1 t},$$

where

$$\begin{aligned} H_{mn}(\omega) &= \frac{1}{T_1}\int_{t_0}^{t_0+T_1} e^{j\gamma(\omega)h(t)}e^{-jn\omega_1 t}\,dt. \\ &= \begin{cases} \frac{e^{-j\gamma(\omega)A}}{j}\left\{\frac{2\gamma(\omega)A\left(e^{j(2\gamma(\omega)A+n\pi)}-1\right)}{4(\gamma(\omega))^2A^2-\pi^2n^2}\right\} & \text{if} \quad 4(\gamma(\omega))^2A^2-\pi^2n^2\neq 0 \\ \frac{e^{-j\gamma(\omega)A}}{2} & \text{if} \quad 4(\gamma(\omega))^2A^2-\pi^2n^2=0 \text{ and } n\neq 0 \\ 1 & \text{if} \quad mA=n=0 \end{cases} \end{aligned}$$

The next step is again to select the values of $\alpha(\omega)$, $\beta(\omega)$ and $\gamma(\omega)$ for the particular sampling method from Table I. The resulting equations for the Fourier coefficients for the three sampling methods are summarized in Table IV. The final step in calculating the spectra for SVM is to substitute the values of $G_{mn}(\omega)$ and $H_{mn}(\omega)$ that apply to the specific sampling method into Eq. (14).

Fig. 11 illustrates how the PWM sidebands are generated through the convolution process under the conditions $M = 0.8$ and $\frac{f_c}{f_0} = 150$ for naturally sampled SVM. Figures 11(a) and (b) show the magnitudes of $G_{mn}(\omega)$ and $H_{mn}(\omega)$, respectively. These were calculated by means of the equations for natural sampling in Table IV. Coefficients $H_{mn}(\omega)$ were calculated for n ranging from -75 to +75. Fig. 11(c) shows the full harmonic spectrum for SVM. Fig. 11(d) again shows the harmonic sidebands for sinusoidal PWM under the same conditions. As in the case of third harmonic injection it is again evident how the convolution of sidebands results in a widening and flattening of the sidebands compared to sinusoidal PWM. As a result the WTHD of the line-to-line voltages for SVM is 0.30% compared to 0.33% for sinusoidal modulation. The magnitude of $H_{mn}(\omega)$ decays much slower as n increases than for third harmonic injection PWM. Fig. 11(c) also shows the fundamental

This article has been accepted for publication in a future issue of this journal, but has not been fully edited. Content may change prior to final publication. Citation information: DOI 10.1109/TPEL.2014.2304677, IEEE Transactions on Power Electronics

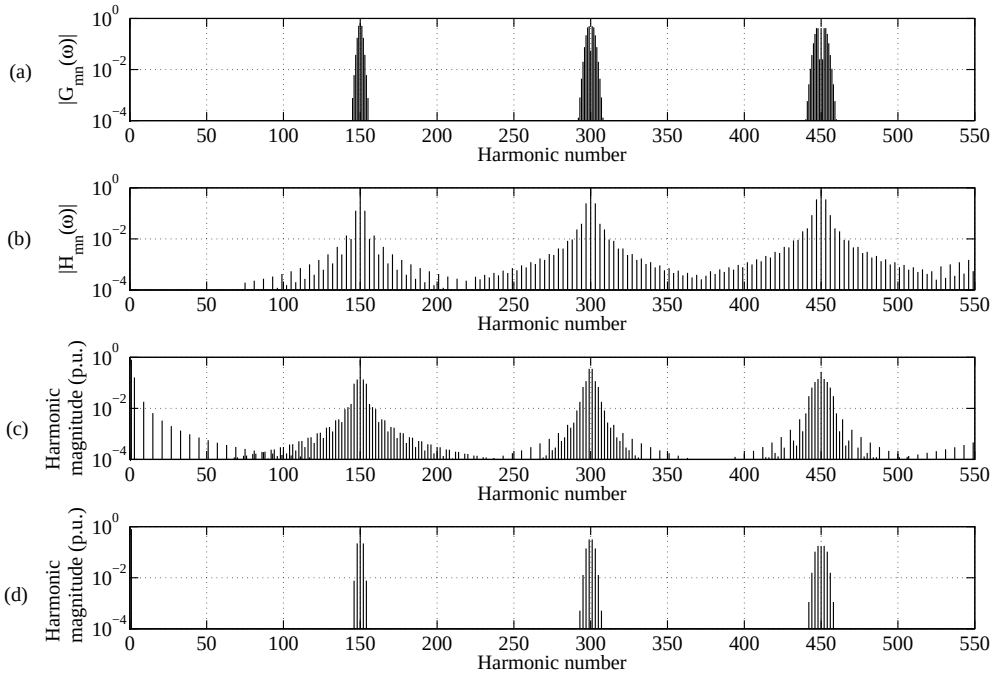

Fig. 11. Generation of the naturally sampled SVM sidebands for $M = 0.8$ and $\frac{f_c}{f_0} = 150$. (a) Absolute value of $G_{mn}(\omega)$ (b) Absolute value of $H_{mn}(\omega)$ (c) Harmonic spectrum of SVM PWM (d) Harmonic spectrum of sinusoidal PWM.

TABLE V

COMPARISON BETWEEN THEORETICAL RESULTS FROM TABLE III, EQUATIONS IN [9] AND FFT OF TIME-DOMAIN SIMULATION

Sampling method	**Error 1 (p.u.)**	**Error 2 (p.u.)**
Natural sampling	5.6e-17	5.7e-6
Symmetric regular sampling	1.6e-16	1.3e-5
Asymmetric regular sampling	1.1e-16	1.2e-5

sinusoidal component as well as the injected third order harmonic components. These harmonics as well as all the sideband harmonics for which n is an integer multiple of three cancel out when calculating the line-to-line voltages.

IX. SPECTRAL RESULTS

In order to verify the validity of the analytic equations derived in this paper the results were numerically compared with the equations in [9] and results from time-domain simulations. A carrier to fundamental frequency ratio of $\frac{f_c}{f_0} = 40$ and a modulation index of $M = 1.1$ is used throughout this section.

Fig. 12 shows the results for third harmonic injection PWM calculated from the equations in Table III. The results from Table III were compared with those from equations (5.43), (5.48) and (5.49) of [9] as well as the FFT of a time-domain simulation. Error 1 in Table V shows the maximum absolute difference between the results from Table III and those from [9] up to the 140'th harmonic. The harmonics generated by the two sets of equations were subtracted as complex numbers before the absolute value of this difference was calculated. This method of comparison would detect errors in both magnitude and phase. Similarly, Error 2 in Table V shows the maximum absolute difference between the results of Table III and the results of the time-domain simulations. All six errors in this Table can seen to be negligible which verifies the validity of the theoretical

This article has been accepted for publication in a future issue of this journal, but has not been fully edited. Content may change prior to final publication. Citation information: DOI 10.1109/TPEL.2014.2304677, IEEE Transactions on Power Electronics

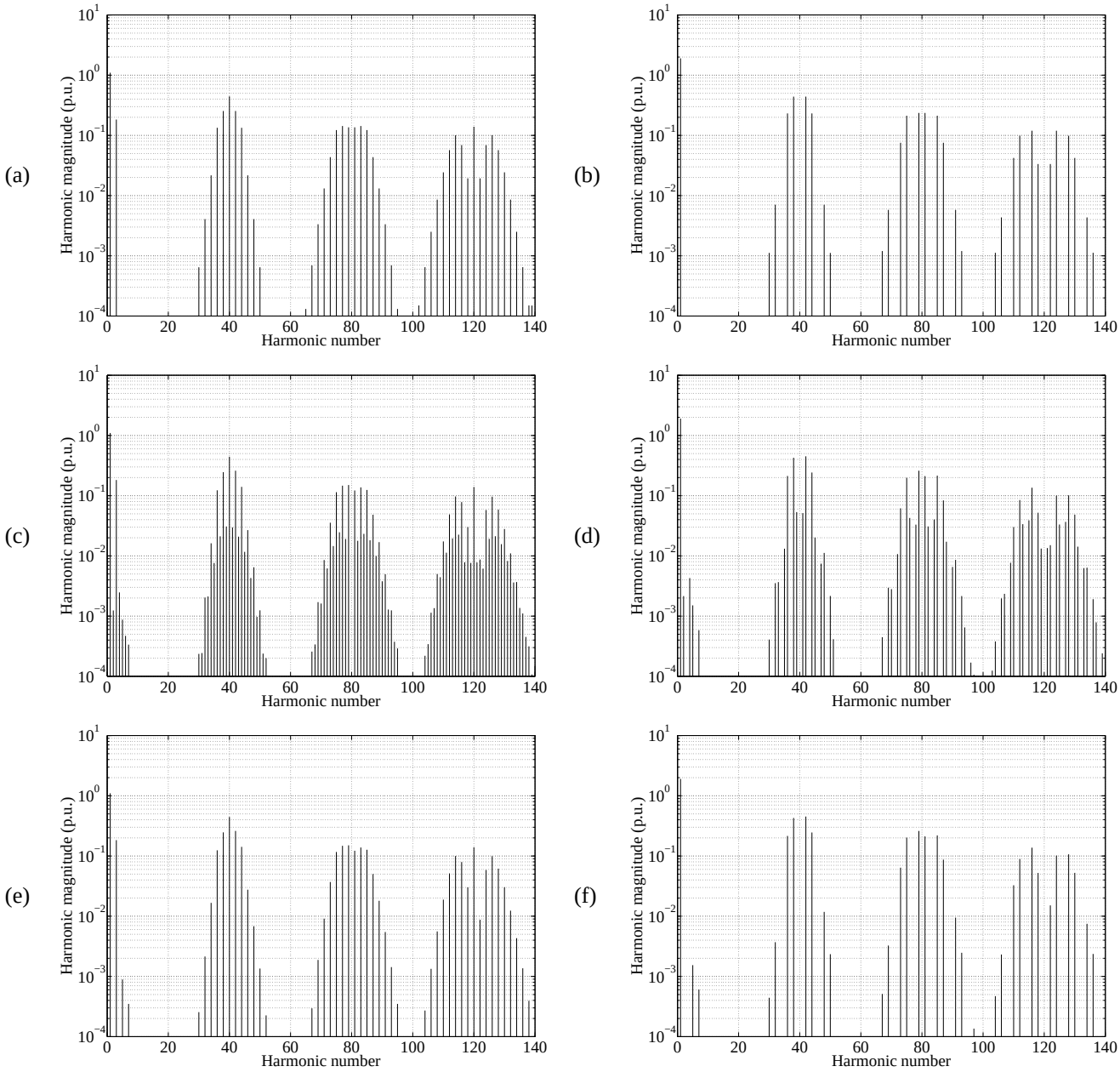

Fig. 12. Theoretical harmonic spectra for third harmonic injection PWM with $M = 1.1$ and $\frac{f_c}{f_0} = 40$. (a) phase leg a natural sampling (b) *l-l natural sampling (c) phase leg a symmetrical regular sampling (d)* l-l symmetrical regular sampling (e) phase leg a asymmetrical regular sampling (f) *l-l asymmetrical regular sampling*

results from this paper for third harmonic injection PWM.

Fig. 13 shows the results for SVM PWM calculated from the equations in Table IV. The results from Table IV were compared with those from equations (6.59), (6.62) and (6.63) of [9] as well as the FFT of a time-domain simulation. As for third harmonic injection Error 1 in Table VI shows the maximum absolute value of the difference between the results from Table IV and those from [9] up to the 140'th harmonic. Although the errors are larger than those in Table V the largest error is still only 0.49%.

This article has been accepted for publication in a future issue of this journal, but has not been fully edited. Content may change prior to final publication. Citation information: DOI 10.1109/TPEL.2014.2304677, IEEE Transactions on Power Electronics

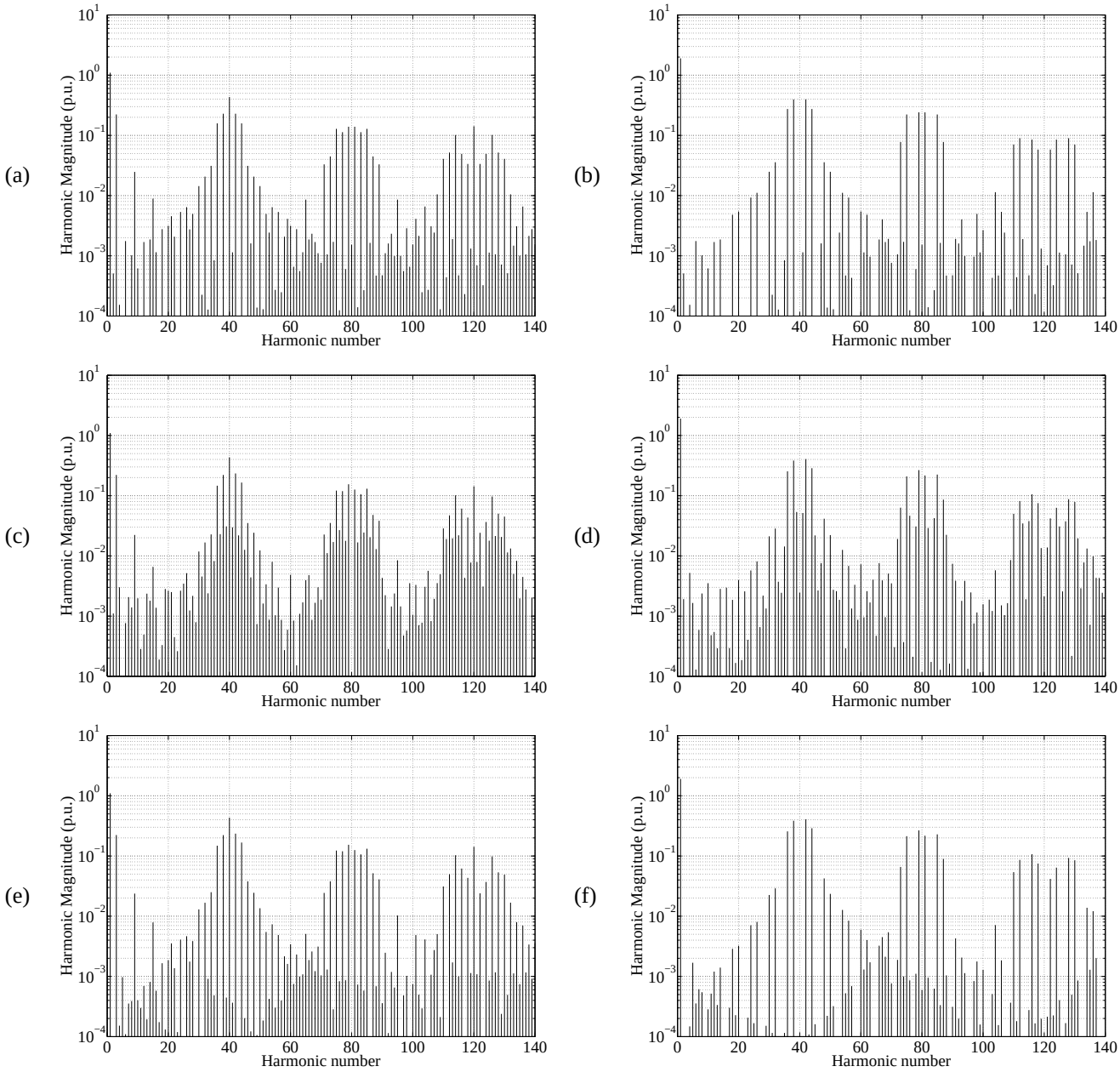

Fig. 13. Theoretical harmonic spectra for space vector modulation PWM with $M = 1.1$ and $\frac{f_c}{f_0} = 40$. (a) phase leg a natural sampling (b) *l-l natural sampling (c) phase leg a symmetrical regular sampling (d)* l-l symmetrical regular sampling (e) phase leg a asymmetrical regular sampling (f) *l-l asymmetrical regular sampling*

X. Conclusions

This paper illustrated how it is possible to use basic mathematical methods to derive expressions for the harmonic spectra of double-edge PWM waveforms. Unlike the cumbersome double Fourier series method, the proposed method does not require the construction of a unit cell for every new reference signal and does not rely on double Fourier series methods. This new approach greatly simplifies the derivations for the analytic spectra of the most common PWM schemes, including sinusoidal, third-harmonic-injection and space-vector modulation. The underlying non-linearity that generates the naturally sampled PWM sidebands was identified. New generalized equations, for the spectra of symmetric regular and asymmetric regular sampled PWM waveforms were derived. These equations apply to both periodic and aperiodic references.

This article has been accepted for publication in a future issue of this journal, but has not been fully edited. Content may change prior to final publication. Citation information: DOI 10.1109/TPEL.2014.2304677, IEEE Transactions on Power Electronics

TABLE VI

COMPARISON BETWEEN THEORETICAL RESULTS FROM TABLE IV, EQUATIONS IN [9] AND FFT OF TIME-DOMAIN SIMULATION

Sampling method	**Error 1 (p.u.)**	**Error 2 (p.u.)**
Natural sampling	0.0034	7.5e-4
Symmetric regular sampling	0.0049	4.6e-4
Asymmetric regular sampling	0.0045	1.4e-4

It was shown that the addition of reference waveforms in the time domain results in a double convolution of sidebands in the frequency domain. A new approach whereby the spectra of naturally sampled, symmetric regular sampled and asymmetric regular sampled PWM waveforms can be calculated through a single process was presented. As an application of the convolution theorem it was shown how new analytic equations for the spectra of third harmonic injection PWM and SVM can easily be derived. Finally the new theoretical results from this paper were benchmarked against those in the literature.

REFERENCES

[1] H. Black, *Modulation Theory*. New York: von Nostrand, 1953.

[2] W. Bennet, "New results in the calculation of modulation products," *Bell System Technical Journal*, vol. 12, pp. 228 – 243, Apr. 1933.

[3] Z. Song and D. V. Sarwate, "The frequency spectrum of pulse width modulated signals," *Signal Processing*, vol. 83, no. 10, pp. 2227 – 2258, 2003. [Online]. Available: http://www.sciencedirect.com/science/article/pii/S0165168403001646

[4] R. Guinee and C. Lyden, "A novel Fourier series time function for modeling and simulation of PWM," *Circuits and Systems I: Regular Papers, IEEE Transactions on*, vol. 52, no. 11, pp. 2427 – 2435, 2005.

[5] A. Leedy, W. Dillard, and R. Nelms, "Harmonic analysis of a two-level sinusoidal PWM inverter using the method of pulse pairs," in *Industrial Electronics Society, 2005. IECON 2005. 31st Annual Conference of IEEE*. IEEE, 2005, pp. 1683–1688.

[6] G. Fedele and D. Frascino, "Spectral analysis of a class of DC–AC PWM inverters by Kapteyn series," *Power Electronics, IEEE Transactions on*, vol. 25, no. 4, pp. 839–849, 2010.

[7] S. M. Cox, "Voltage and current spectra for a single-phase voltage source inverter," *IMA Journal of Applied Mathematics*, vol. 74, no. 5, pp. 782–805, 2009.

[8] D. Kostic, Z. Avramovic, and N. Ciric, "A new approach to theoretical analysis of harmonic content of PWM waveforms of single- and multiple-frequency modulators," *Power Electronics, IEEE Transactions on*, 2012.

[9] D. Holmes and T. Lipo, *Pulse Width Modulation for Power Converters (Principles and Practice)*. IEEE Press Series on Power Engineering, 2003.

[10] D. Holmes and B. McGrath, "Opportunities for harmonic cancellation with carrier-based PWM for a two-level and multilevel cascaded inverters," *Industry Applications, IEEE Transactions on*, vol. 37, no. 2, pp. 574 –582, Mar/Apr 2001.

[11] R. Wilkinson, T. Meynard, and H. du Toit Mouton, "Natural balance of multicell converters: The two-cell case," *Power Electronics, IEEE Transactions on*, vol. 21, no. 6, pp. 1649 –1657, Nov. 2006.

[12] ——, "Natural balance of multicell converters: The general case," *Power Electronics, IEEE Transactions on*, vol. 21, no. 6, pp. 1658 –1666, Nov. 2006.

[13] B. McGrath and D. Holmes, "Enhanced voltage balancing of a flying capacitor multilevel converter using phase disposition (PD) modulation," *Power Electronics, IEEE Transactions on*, vol. 26, no. 7, pp. 1933 –1942, July 2011.

[14] ——, "Analytical modelling of voltage balance dynamics for a flying capacitor multilevel converter," *Power Electronics, IEEE Transactions on*, vol. 23, no. 2, pp. 543 –550, March 2008.

[15] ——, "Analytical determination of the capacitor voltage balancing dynamics for three-phase flying capacitor converters," *Industry Applications, IEEE Transactions on*, vol. 45, no. 4, pp. 1425 –1433, July-Aug. 2009.

[16] ——, "Natural capacitor voltage balancing for a flying capacitor converter induction motor drive," *Power Electronics, IEEE Transactions on*, vol. 24, no. 6, pp. 1554 –1561, June 2009.

[17] A. Shukla, A. Ghosh, and A. Joshi, "Natural balancing of flying capacitor voltages in multicell inverter under PD carrier-based pwm," *Power Electronics, IEEE Transactions on*, vol. 26, no. 6, pp. 1682 –1693, June 2011.

[18] S. Thielemans, A. Ruderman, B. Reznikov, and J. Melkebeek, "Improved natural balancing with modified phase-shifted pwm for single-leg five-level flying-capacitor converters," *Power Electronics, IEEE Transactions on*, vol. 27, no. 4, pp. 1658–1667, 2012.

This article has been accepted for publication in a future issue of this journal, but has not been fully edited. Content may change prior to final publication. Citation information: DOI 10.1109/TPEL.2014.2304677, IEEE Transactions on Power Electronics

[19] H. d. T. Mouton and B. Putzeys, "Understanding the PWM nonlinearity: Single-sided modulation," *Power Electronics, IEEE Transactions on*, vol. 27, no. 4, pp. 2116 – 2128, Apr. 2012.

[20] S. Bowes, "New sinusoidal pulsewidth modulated inverter," *Proceedings IEE*, vol. 122, no. 11, pp. 1279 –1285, 1975.

[21] D. Holmes, "A general analytical method for determining the theoretical harmonic components of carrier based PWM strategies," in *Industry Applications Conference, 1998. Thirty-Third IAS Annual Meeting. The 1998 IEEE*, vol. 2, Oct. 1998, pp. 1207 –1214 vol.2.

[22] Heng, L. Helle, Y. Bo, and K. Larsen, "A general solution for theoretical harmonic components of carrier based PWM schemes," in *Applied Power Electronics Conference and Exposition, 2009. APEC 2009. Twenty-Fourth Annual IEEE*, Feb. 2009, pp. 1698 –1703.

[23] A. Oppenheim, W. Schafer, and J. Buck, *Discrete-time signal processing*. Prentice Hall, 1998.

[24] J. Goldberg and M. Sandler, "Pseudo-natural pulse width modulation for high accuracy digital-to-analogue conversion," *Electronics Letters*, vol. 27, no. 16, pp. 1491 –1492, Aug. 1991.

[25] B. Putzeys, "Simple, ultralow distortion digital pulse width modulator," in *Audio Engineering Society Convention 120*, 5 2006. [Online]. Available: http://www.aes.org/e-lib/browse.cfm?elib=13498

[26] J.-W. Jung and M. Hawksford, "An oversampled digital PWM linearization technique for digital-to-analog conversion," *Circuits and Systems I: Regular Papers, IEEE Transactions on*, vol. 51, no. 9, pp. 1781 – 1789, Sep 2004.

[27] A. Saichev and W. Woyczynski, *Distributions in the Physical and Engineering Sciences, Volume 1: Distributional and Fractal Calculus, Integral Transforms and Wavelets*, ser. Applied and Numerical Harmonic Analysis. Birkhäuser Boston, 1996.

[28] G. Watson, *Theory of Bessel Functions*. Cambridge University Press, 1944.

[29] I. Deslauriers, N. Avdiu, and B. T. Ooi, "Naturally sampled triangle carrier PWM bandwidth limit and output spectrum," *Power Electronics, IEEE Transactions on*, vol. 20, no. 1, pp. 100 – 106, Jan. 2005.

[30] M. Odavic, M. Sumner, P. Zanchetta, and J. Clare, "A theoretical analysis of the harmonic content of PWM waveforms for multiple-frequency modulators," *Power Electronics, IEEE Transactions on*, vol. 25, no. 1, pp. 131 –141, Jan 2010.

[31] D. Champeney, *A handbook of Fourier theorems*. Cambridge: Cambridge University Press, 1987.

[32] J. A. Houldsworth and D. A. Grant, "The use of harmonic distortion to increase the output voltage of a three-phase PWM inverter," *Industry Applications, IEEE Transactions on*, vol. IA-20, no. 5, pp. 1224 –1228, Sep. 1984.

[33] H. van der Broeck, H.-C. Skudelny, and G. Stanke, "Analysis and realization of a pulsewidth modulator based on voltage space vectors," *Industry Applications, IEEE Transactions on*, vol. 24, no. 1, pp. 142 –150, Jan/Feb 1988.

[34] S. Bowes and Y.-S. Lai, "The relationship between space-vector modulation and regular-sampled PWM," *Industrial Electronics, IEEE Transactions on*, vol. 44, no. 5, pp. 670 –679, Oct 1997.

[35] J. Boys and P. Handley, "Harmonic analysis of space vector modulated PWM waveforms," *Electric Power Applications, IEE Proceedings B*, vol. 137, no. 4, pp. 197 –204, Jul. 1990.

[36] D. Holmes, "The general relationship between regular-sampled pulse-width-modulation and space vector modulation for hard switched converters," in *Industry Applications Society Annual Meeting, 1992., Conference Record of the 1992 IEEE*, Oct 1992, pp. 1002 –1009 vol.1.

[37] A. Kwasinski, P. Krein, and P. Chapman, "Time domain comparison of pulse-width modulation schemes," *Power Electronics Letters, IEEE*, vol. 1, no. 3, pp. 64 – 68, Sep. 2003.

[38] D. Holmes, "The significance of zero space vector placement for carrier-based PWM schemes," *Industry Applications, IEEE Transactions on*, vol. 32, no. 5, pp. 1122 –1129, Sep/Oct 1996.

PLACE PHOTO HERE

Hendrik du T. Mouton (S'98-M'00) received the B.Sc., B.Sc.Hons, M.Sc., and Ph.D. in mathematics degrees from the University of the Orange Free-state in 1986, 1987, 1988 and 1991, respectively and the B.Eng and Ph.D. degrees in Electrical Engineering from the University of Stellenbosch in 1996 and 2000, respectively. He is currently a Professor in electrical Engineering at the University of Stellenbosch and leader of the Power Electronics Research Group. He authored and co-authored a number of international journal and conference papers in mathematics and in power electronics. His research interests include multilevel converters, utility applications of power electronics and class-d audio amplifiers.

This article has been accepted for publication in a future issue of this journal, but has not been fully edited. Content may change prior to final publication. Citation information: DOI 10.1109/TPEL.2014.2304677, IEEE Transactions on Power Electronics

PLACE PHOTO HERE

Brendan McGrath (M99) received the BE degree in Electrical and Computer Systems Engineering (1997), the BSc degree in Applied Mathematics and Physics (1997), and the Ph.D. degree (2003) from Monash University, Victoria, Australia. Dr McGrath is with the school of electrical and computer engineering at RMIT university in Melbourne Australia. He has previously held positions at Monash University (2007-2010) and the University of Newcastle (2005-2006) both in Australia. Prior to this he was a post-doctoral researcher with the Laboratoire dElectrotechnique et dElectronique Industrielle (LEEI), Toulouse, France. His research interests include the modulation and control of power electronic converters, with a particular emphasis on multilevel conversion systems. He has published over 60 journal and conference articles, and in 2004 was awarded the Douglas Lampard research medal from Monash University for his Ph.D. thesis. Dr McGrath is a member of the IEEE Power Electronics, Industry Applications and Industrial Electronics Societies, and is an associate editor for the IEEE Transactions on Industry Applications and the IEEE Transactions on Industrial Informatics.

PLACE PHOTO HERE

Donald Grahame Holmes (M88SM03-F13) received the B.S. and M.S. degrees in power systems engineering from the University of Melbourne, Melbourne, Australia, in 1974 and 1979, respectively, and the Ph.D. degree in PWM theory for power electronic converters from Monash University, Clayton, Australia, in 1998. In 1984, he joined Monash University, where he established and directed the Power Electronics Group for over 25 years. In 2010, he moved to RMIT University, Melbourne, to take up a professorial chair in Smart Energy. He has a strong commitment and interest in the control and operation of electrical power converters. His research interests include fundamental modulation theory and its application to the operation of energy conversion systems, current regulators for drive systems and PWM rectifiers, active filter systems for the quality of supply improvement, resonant converters, current-source inverters for drive systems, and multilevel converters. He has made a significant contribution to the understanding of PWM theory through his publications and has developed close ties with the international research community in the area. He has published over 200 papers at international conferences and in professional journals and regularly reviews papers for all major IEEE TRANSACTIONS in his area. He has also coauthored a major reference textbook on PWM theory with Prof. Thomas Lipo of the University of Wisconsin-Madison. Prof. Holmes is an active member of the Industrial Power Converter and Industrial Drives Committees of the IEEE Industry Applications Society and is an active member of the IEEE Power Electronics Society AdCom.

PLACE PHOTO HERE

Richardt H. Wilkinson (S97M05SM'11) was born in Vereeniging, South Africa, in 1972. He received the B.Eng., M.Eng., and Ph.D. degrees from the University of Stellenbosch, Stellenbosch, South Africa, in 1994, 1998, and 2004, respectively. He joined the Cape Peninsula University of Technology in Cape Town, South Africa as a Postdoctoral Researcher in 2005, after which he was appointed as Senior Researcher in 2007. In 2008 he was appointed as the Head of the Centre for Instrumentation Research and promoted to Associate Professor in 2011. He joined RMIT University in Melbourne, Australia in 2012, where he is currently a Senior Lecturer in the School of Electrical and Computer Engineering. His research interests include multilevel power electronic converters, modulation techniques, Fourier techniques, digital signal processing, digital audio amplifiers, FPGA development, and embedded controller design. Dr. Wilkinson is an active Member of the IEEE Power Electronics, Industry Applications, Industrial Electronics, and Power Engineering Societies. He served as Chapter Chair for the South Africa Section's Joint Industry Applications/Industrial Electronics/Power Electronics Chapter from 2007 to 2012.